JVST B
Journal of Vacuum Science & Technology B

Low-temperature chemical vapor deposition growth of graphene films enabled by ultrathin alloy catalysts

Cite as: J. Vac. Sci. Technol. B **38**, 032202 (2020); https://doi.org/10.1116/1.5144692
Submitted: 09 January 2020 . Accepted: 09 March 2020 . Published Online: 31 March 2020

Samuel Olson, Otto Zietz, Joshua Tracy, Yanlong Li, Chenggang Tao, and Jun Jiao

JVST B
Journal of Vacuum Science & Technology B

ARTICLE

avs.scitation.org/journal/jvb

Low-temperature chemical vapor deposition growth of graphene films enabled by ultrathin alloy catalysts

Cite as: J. Vac. Sci. Technol. B 38, 032202 (2020); doi: 10.1116/1.5144692
Submitted: 9 January 2020 · Accepted: 9 March 2020 ·
Published Online: 31 March 2020

Samuel Olson,[1] Otto Zietz,[1] Joshua Tracy,[1] Yanlong Li,[2] Chenggang Tao,[2] and Jun Jiao[1,a)]

AFFILIATIONS

[1]Department of Mechanical and Materials Engineering, Portland State University, 1930 SW 4th Ave., Portland, Oregon 97201
[2]Department of Physics, Virginia Polytechnic Institute, 850 W Campus Drive, Blacksburg, Virginia 24061

[a)]**Author to whom correspondence should be addressed:** jiaoj@pdx.edu

ABSTRACT

This report introduces a method for fabricating graphene at low temperatures via chemical vapor deposition enabled by ultrathin (~1 nm) nickel-gold (Ni-Au) catalysts. The unique combination of high carbon (C) solubility Ni, low C solubility Au, and an ultrathin layer of a catalyst demonstrates the effectiveness to produce graphene at 450 °C with the layer number independent of growth duration. In contrast to grain-boundary defined catalyst morphology found in thicker (>20 nm) metal catalysts, the ultrathin catalyst morphology leads to the formation of nanoscale metal "islands" during the growth process, which results in curved graphene covering the catalyst. To test the effect of preactivation of the ultrathin catalyst for the formation of graphene, a preanneal process of the catalyst followed by the introduction of a carbon precursor was also investigated. The preanneal process resulted in the formation of carbon nanotubes (CNTs) in lieu of graphene, displaying the impact of the catalytic surface treatment in relation to the produced materials. The results and discussion presented here detail a low-temperature nanoscale manufacturing process that allows for the production of either graphene or CNTs on an ultrathin catalyst.

I. INTRODUCTION

Graphene, a single atomic layer of sp^2 hybridized carbon atoms, has developed a large amount of interest since its isolation in 2004.[1] Its outstanding mechanical,[2,3] electrical,[4–6] and optical[7–9] properties promise applicability in a wide array of engineering fields. Graphene has applications in energy storage (supercapacitors[10] and batteries[11]), energy generation (fuel cells[12]), sensing (glucose,[13] CO_2,[14] etc.[15–17]), and nanoelectronics, which, in particular, has arisen as one of the most potentially impactful applications of the material. Graphene-based field effect transistors have shown improvements over traditional silicon-based MOSFETs in high-frequency applications[18–21] due to graphene's high carrier mobility.[22,23] Graphene has also been shown to exhibit superior heat dissipation properties in electronic applications.[24] In order to take advantage of these properties, it is necessary to design a fabrication process for direct or near-direct growth on the targeted substrate at a reasonably low temperature to avoid damage to the surrounding substrate. Several groups have demonstrated the ability of graphene to perform as an excellent barrier to diffusion of both gaseous and metallic materials.[25,26] These properties have produced significant interest as a solution to common failure modes involving diffusion related degradation in nanoscale electronics. In these applications, a single layer is necessary due to the scale of the features involved. If direct conformal growth of graphene on arbitrary features for use as a diffusion barrier is required, low temperature growths must be employed to avoid further diffusion and degradation of the materials.

Initially isolated using micromechanical cleavage, various graphene fabrication methods have since been developed. These methods include chemical exfoliation,[27] thermal decomposition of carbon-containing compounds,[28] and numerous chemical vapor deposition (CVD) methods.[29,30] Chemical exfoliation has the benefit of being relatively cheap and low-temperature; however, it is difficult to obtain large platelets of monolayer graphene. Additionally, direct growth of graphene onto surfaces is not feasible with this growth method, limiting final target substrates to

two-dimensional surfaces. Graphene fabrication via thermal decomposition, typically of SiC, exhibits high growth controllability; however, exceedingly high temperatures and small grain sizes make this method unattractive for electronic applications. CVD growth methods present perhaps the most promising avenue toward the incorporation of graphene into the modern electronics industry due to their ability to produce high quality, monolayer sheets in a scalable and cost-effective manner. The basis of the CVD growth process involves decomposition of a carbon-containing molecule on the surface of a transition metal catalyst. The two most common catalysts are the transition metals Cu[31–33] and Ni.[34–36] A major roadblock preventing large-scale incorporation of CVD-fabricated graphene into industry processes is the excessively high temperatures required for monolayer growth. Cu catalyst substrates yield majority monolayer graphene through a self-limiting surface reaction, but the temperature required for growth is upward of 800 °C for gaseous carbon precursors such as methane and acetylene.[37,38] Researchers have had success lowering the growth temperature of Cu by exchanging the aforementioned gaseous carbon precursors for a molecule that already possesses an aromatic ring such as toluene, but growth temperatures remain above 600 °C.[39] The required growth temperature reduces drastically if an Ni catalyst is used instead, but the high carbon solubility of Ni leads to the catalyst acting as a large reservoir for carbon that precipitates out upon cooling, making layer number control difficult.[40] Despite this, the lower energy barrier of graphene formation on Ni catalysts has resulted in researchers studying the effect of catalyst composition and morphology on growth characteristics. Multimetal layered catalysts such as Ni/Mo or Ni/Au display reduced layer number at lower growth temperatures, but a higher temperature anneal and thick catalyst are still required for such a growth.[41,42] The thickness of these catalysts presents another challenge to the incorporation of graphene in the industry. These catalysts are too bulky to have applications in nanoscale devices and so require a post-growth transfer to the target substrate. Current transfer methods often result in tears in the graphene film and limit the final target substrate to a planar geometry if the defect density is to remain

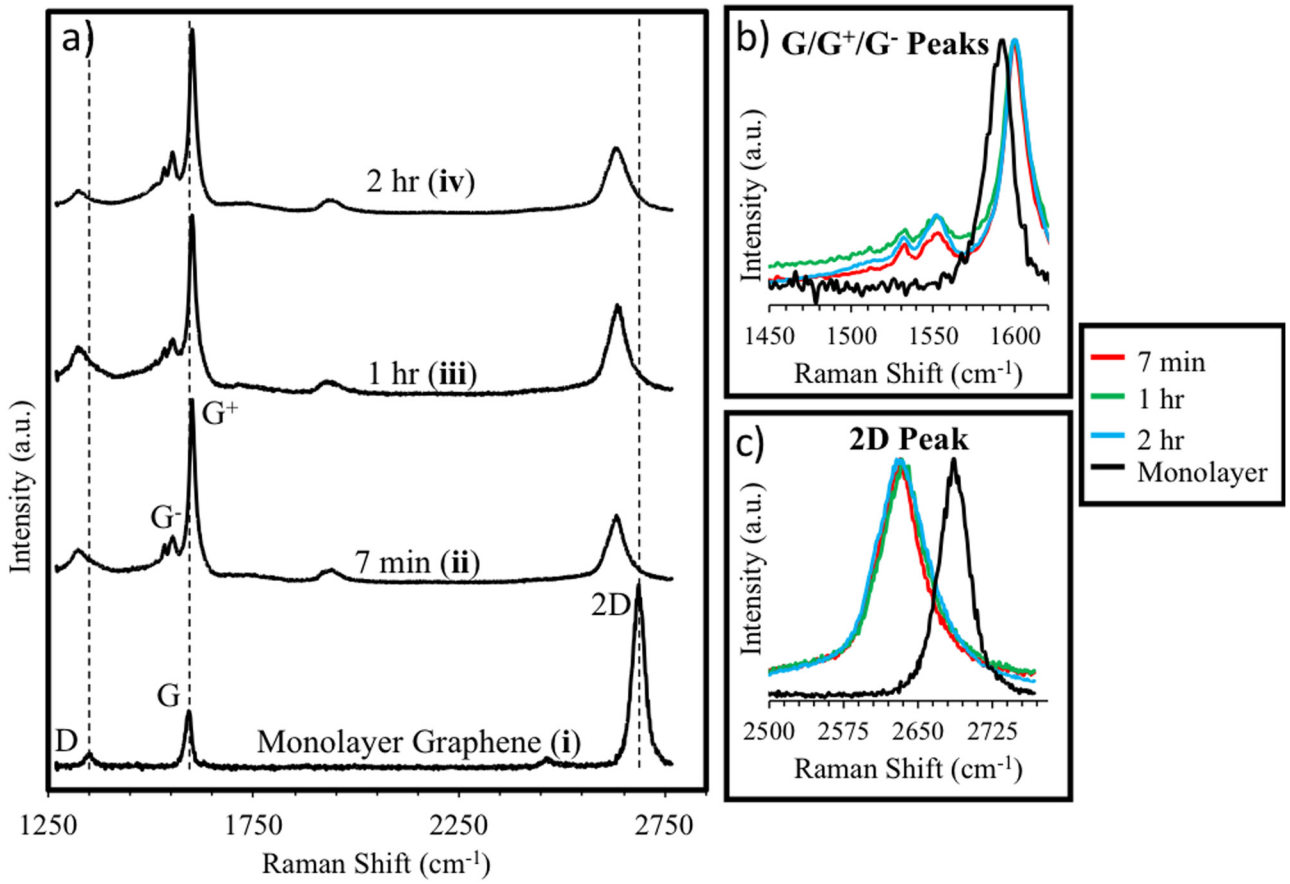

FIG. 1. (a) Averaged Raman spectra of 7 min (ii), 1 h (iii), and 2 h (iv) growths on 1 nm Ni/Au catalyst, and a monolayer graphene Raman spectrum (i) for comparison (grown on 1.5 μm Cu at 750 °C). Dashed lines indicate positions of D, G, and 2D peaks in monolayer graphene. (b) Comparison of G peaks of all four growths, with all 1 nm grown spectra normalized to the G^+ peak. (c) Comparison of normalized 2D peaks of all four growths.

low.[43,44] Our previous studies have shown that when catalyst metals are premixed and codeposited rather than layered on top of one another to form the catalyst surface, the subsequent graphene growths proceed in a slower and more controllable fashion at lower temperatures without the need for a high-temperature preanneal.[45,46] These studies also demonstrate the ability of added Au to promote layer number control and to shift the growth mechanism from absorption-precipitation (as is standard for pure Ni catalysts) to surface-dominated. In this research, we present CVD-fabricated graphene grown on a 1 nm thick codeposited Ni/Au catalyst at 450 °C. The properties of both the graphene and the catalyst are analyzed postgrowth to determine physical, chemical, and morphological properties.

II. METHODS

The ultrathin Ni/Au film was fabricated via electron-beam evaporation. A mixture of 99 wt. % Ni and 1 wt. % Au pellets was prepared in a graphite crucible. This crucible was then placed in a KJL AXXIS physical vapor deposition system, where the Ni/Au mixture was melted and evaporated onto 300 nm oxide Si wafers, a process we have used previously with thicker catalysts.[45] The coated wafers were then placed in a custom-built cold-wall CVD reactor with a radiatively heated stage. A thermocouple was affixed directly onto the surface of the catalyst to allow for precise measurement of the catalyst temperature during the growth process. The CVD chamber was evacuated to a pressure of $\sim 1 \times 10^{-2}$ Torr using a rough pump, after which the wafer was heated to 450 °C under 15 SCCM H_2. Upon reaching growth temperature, the H_2 flow was ceased, and 0.1 SCCM C_2H_2 was introduced to the chamber. C_2H_2 was chosen as the carbon feedstock due to its ability to lower defect density in graphene.[47] The temperature and the C_2H_2 flow rate were maintained for variable amounts of time. The graphene films were transferred to TEM grids by etching the underlying SiO_2 with potassium hydroxide (KOH).

To test the impact of preannealing on the catalyst, growths were conducted wherein the catalyst was held at growth temperature for several minutes prior to the introduction of the carbon precursor. This growth method was found to produce carbon nanotubes (CNTs). The as-grown graphene and CNTs were analyzed using Raman spectroscopy (Horiba HR800 UV, with 100 mW 532 nm excitation laser and 10 s acquisition periods averaging five times). Peak full-width-half-maxima (FWHM) and locations were analyzed using Fityk peak-fitting software. The catalyst morphologies were analyzed using scanning electron microscopy (SEM) and atomic force microscopy (AFM). AFM measurements were carried out on a Bruker Dimension Icon at atmosphere, with topography images captured via a SCANASYST-AIR probe with a nominal frequency of 70 kHz, a spring constant of 0.4 N m^{-1}, and a nominal tip radius of 2 nm.

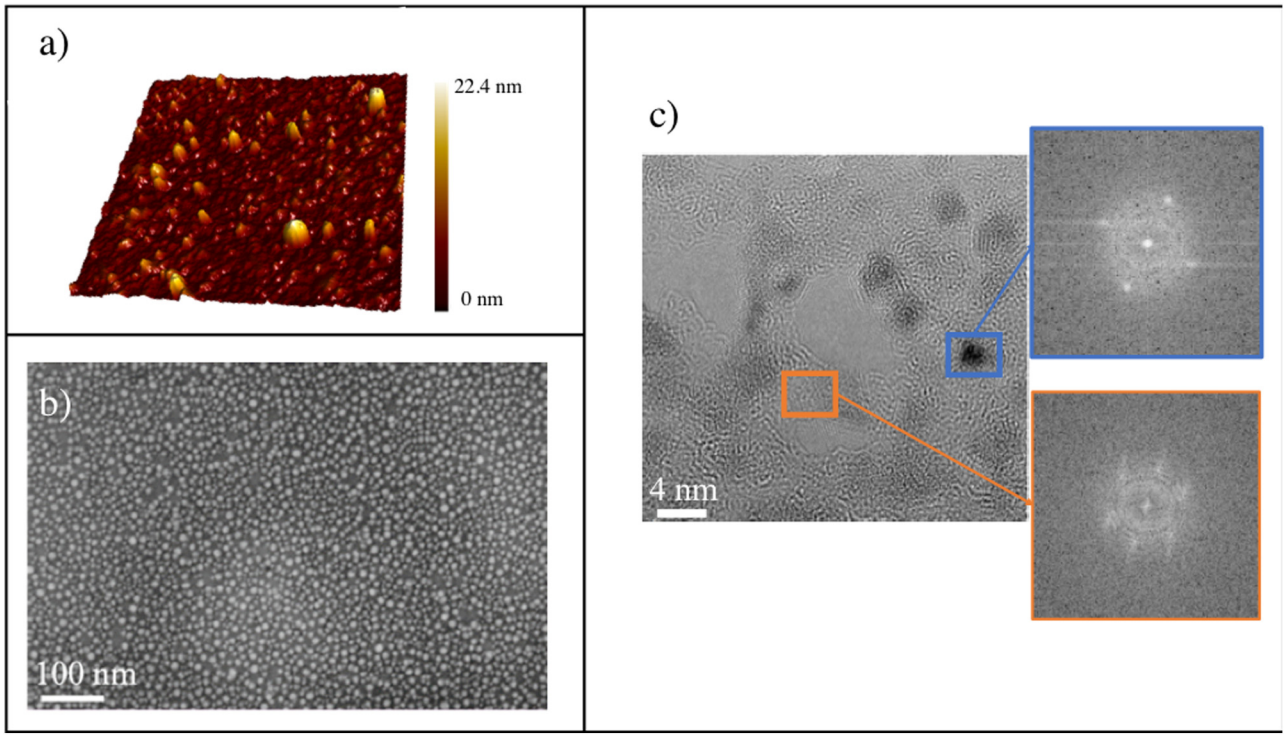

FIG. 2. (a) AFM topographical map of a 1 nm catalyst postgrowth (1 × 1 μm^2). (b) SEM micrograph of the surface postgrowth. (c) TEM micrograph of the transferred 1 nm catalyst, with callouts showing FFT of cubic (top) and hexagonal (bottom) crystalline regions. Growth duration for all images is 7 min.

III. RESULTS AND DISCUSSION

Upon successful deposition of the catalyst, it was necessary to design an experiment involving varying growth times to observe the effect on the outcome of the graphene on this unique catalyst. Standard CVD graphene growth durations range between 1 min and 1 h. Following prior successful CVD growths on thicker codeposited catalysts with a 7 min growth, this became the starting point for assessing the 1 nm catalyst.[45] Subsequently, longer growths were conducted to analyze the effect of extended carbon precursor exposure. The sample surfaces were analyzed via Raman spectroscopy upon completion of the CVD growth.

Graphene has three main Raman peaks: D, G, and 2D. The D peak (~1350 cm^{-1}) arises from defects in the graphene lattice and is not observed in pristine graphene.[48,49] The G peak (~1590 cm^{-1}) is caused by a doubly degenerate mode, E_{2g}, which is observed in all graphene samples.[49,50] The 2D peak (~2680 cm^{-1}) is the second order D peak but does not require a defect in the lattice to occur for observation.[48–50] Figure 1(a)(ii)–(a)(iv) shows Raman spectra of the surface of the 1 nm catalyst after 7 min, 1 h, and 2 h growths, with monolayer 1.5 μm Cu-grown graphene for reference [Fig. 1(a)(i)]. Note that there is a clear splitting of the G peak, which occurs due to a breaking of planar symmetry that splits the degenerate modes of E_{2g} into two distinct modes termed G^- and G^+.[50,51] In addition, all three major peaks (D, G, and 2D) are shifted down in wavenumber from the tabulated planar graphene values mentioned above. Peak shifting can be induced by a strain in the graphene lattice, which causes a change in phonon interaction energies.[52] This peak shifting is evident when the Raman spectra of the 1 nm growths are compared to a monolayer graphene Raman spectrum (grown on 1.5 μm Cu at 750 °C). The graphene grown on the 1 nm catalyst displays uniform Raman characteristics over long durations with a change in the FWHM of the 2D peak of 51.56 cm^{-1} at 7 min growth duration to 66.46 cm^{-1} after 2 h of growing. This indicates a consistent layer number even at extended growth times. In contrast, thicker Ni catalysts will continue to produce additional layers of graphene if subjected to extended growth durations due to the nature of the absorption-precipitation growth mechanism. In thicker catalysts, the physical reservoir present for storing carbon during the growth process at temperature is at least 50 times the catalyst thickness here and so has the potential to store much more carbon that will be precipitated out as graphene layers upon cooling as the solubility of carbon in Ni drops with temperature.

Figure 1(b) demonstrates the G peak splitting that occurs in growths completed on the 1 nm catalyst. The G^+ peak consistently occurs at 1600 cm^{-1} for all growth durations and possesses a very small FWHM (<25 cm^{-1}). The G^- peak of the 1 nm catalyst growths also presents consistently at 1552 cm^{-1} through extended growth durations. In contrast, the monolayer graphene presents a thin, single G peak centered at 1590 cm^{-1}. Analysis of the 2D peak

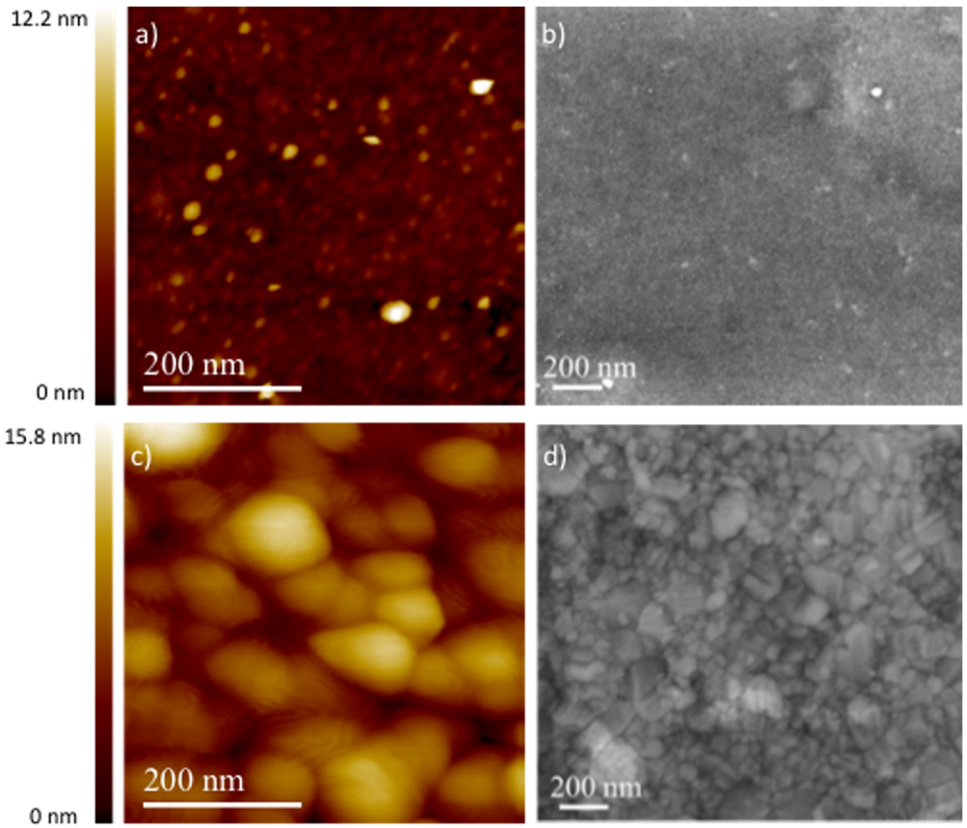

FIG. 3. (a) AFM and (b) SEM images of a 1 nm catalyst postgrowth, displaying catalyst islands. (c) AFM and (d) SEM images of 30 nm catalyst showing the grain structure typical of thicker catalysts. Both growths were 7 min in duration at 450 °C.

in Fig. 1(c) shows a clear shifting of about 52–58 cm^{-1} for the 1 nm catalyst growths compared to a more typical monolayer graphene growth.

Analysis of the catalyst morphology postgrowth reveals island-like nanoparticles that form underneath the graphene (Fig. 2). Upon heating to 450 °C during the growth, the 1 nm catalyst transforms from a continuous thin film to an expanse of nanoscale islands. Topographic AFM analysis of the surface postgrowth [Fig. 2(a)] provides the relative heights of the islands. The islands are 1–3 nm in height on average, with a diameter between 10 and 20 nm. Figure 2(b) shows a high-magnification SEM micrograph of the catalyst surface postgrowth, depicting widespread distribution of the nanoislands, with areas of bare SiO_2 in between. The graphene and 1 nm metal catalyst were transferred to TEM grids postgrowth. A film of poly-(methyl methacrylate) (PMMA) was spun onto the growth wafer, which was then placed in KOH. The KOH etches the SiO_2 layer, allowing the PMMA/graphene film to release and float on the surface. This film was then placed on a copper TEM grid on a small wafer of clean SiO_2. After heating the assembly to 140 °C for 10 min, the wafer was placed in acetone, which removed the PMMA and left only the copper TEM grid with graphene and metal catalyst islands remaining. The resulting TEM micrograph [Fig. 2(c)] shows the graphene film (light gray) with interspersed metal islands (dark gray/black). The callouts display fast Fourier transform (FFT) images of cubic crystallinity on the metal catalyst island areas (top) and hexagonal crystallinity in the graphene film (bottom).

The 1 nm catalyst displays a postgrowth surface morphology drastically different from that found on thicker CVD growth catalysts. The islands observed in the AFM and SEM of the 1 nm

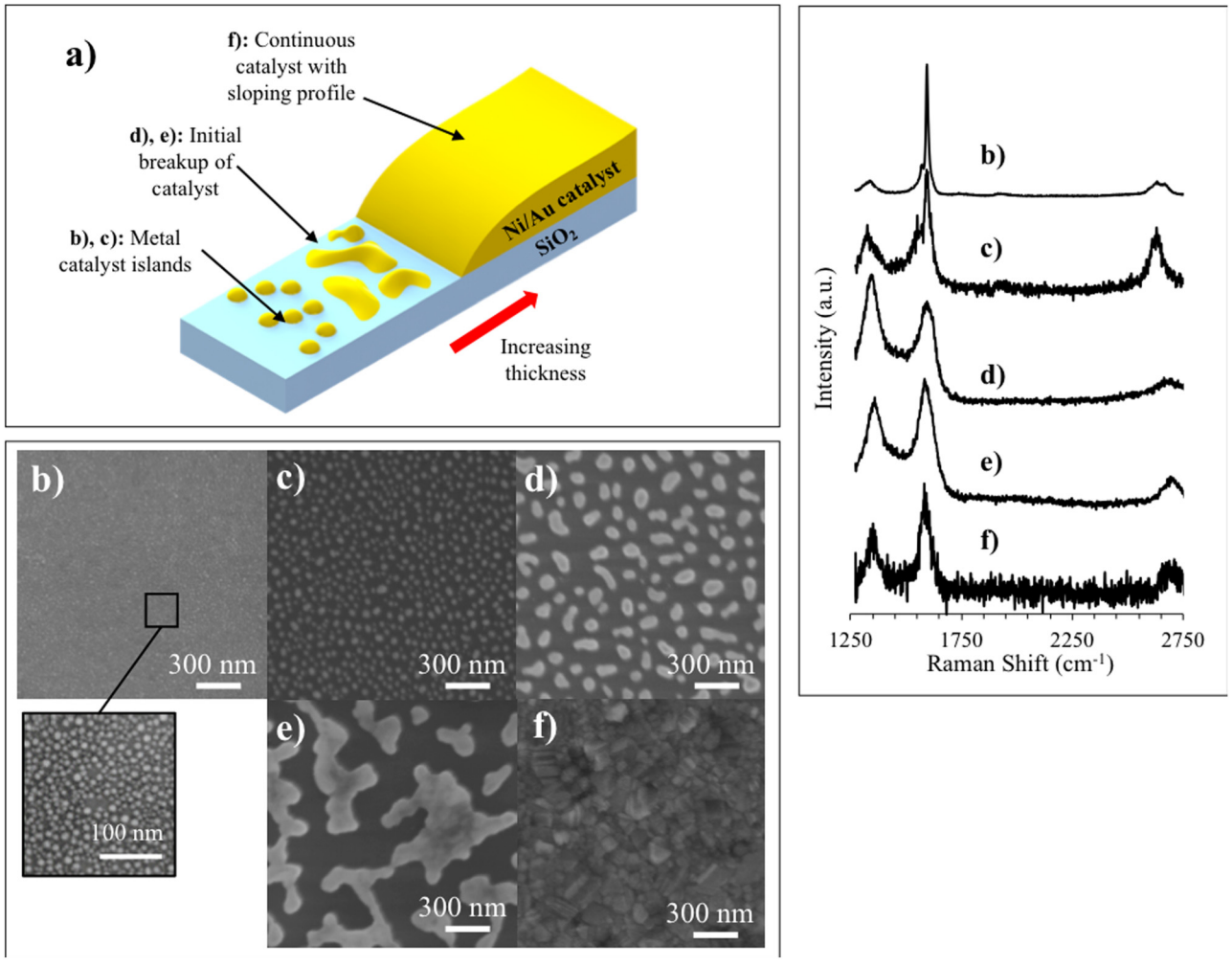

FIG. 4. (a) Thickness gradient mechanism. (b)–(f) SEM micrographs of increasing catalyst thickness. The Raman spectra to the right depict characteristic spectra from the areas in the corresponding SEM micrographs.

catalyst postgrowth [Figs. 3(a) and 3(b)] show stark contrast when compared to AFM and SEM analyses of a more typical 30 nm Ni/Au growth catalyst [Figs. 3(c) and 3(d)]. The 30 nm catalyst displays a typical grain structure with grain diameters on the order of tens of nanometers.

The graphene grown is highly dependent upon catalyst thickness. Figure 4 shows the drastic change in the Raman spectrum traversing from 50 nm Ni/Au to bare SiO_2 along a thickness gradient. The gradient was produced by placing a mask suspended roughly 5 mm over the SiO_2 wafer during initial catalyst deposition. Figure 4(a) is a schematic graph and provides a visual representation of the gradient mechanism, with a zone of roughly 50 nm Ni/Au tapering to a minimal and discontinuous surface. Figures 4(b)–4(f) show SEM micrographs of regions with increasing thickness, with corresponding Raman spectra taken from the same area. Initially, the Raman spectrum on 50 nm Ni/Au [Fig. 4(f)] is typical of a pretransfer Ni growth, displaying a noisy signal with a quenched 2D peak. The SEM micrograph is also typical of thicker catalysts, as a traditional grain structure is observed. As the catalyst becomes thinner, the 2D:G ratio decreases, indicating an increased layer number. This is due to the inability of the carbon atoms to diffuse away and limit graphene growth. The SEM micrographs [Figs. 4(d) and 4(e)] show the catalyst beginning to break up into larger islands of several hundred nanometers in diameter. Figure 4(c) shows circular islands akin to what is observed in the ultrathin region, but the islands (with a diameter of ~40–50 nm) are too large to produce a clean Raman signal, free of fluorescence from the metal substrate. The transition completes once the catalyst is thin enough to form metal islands [Fig. 4(b)], and the Raman signal displays the aforementioned characteristics. The ability of the graphene to grow on ultrathin catalysts presents a potential avenue for direct growth on three-dimensional substrates for diffusion barrier applications.

Although the Raman spectra share some similarities with that of the carbon nanotube (see Fig. 5 below), no such structures were found in studies of the initial postgrowth surfaces with SEM, TEM, or AFM. However, if the catalyst is annealed prior to introduction of a carbon source, CNTs are observed. Figure 5(a) shows an SEM micrograph of a 7 min growth conducted after a 15 min anneal at 450 °C, showing CNTs roughly 20–150 nm in length covering the surface of the catalyst. A growth time of 7 min was chosen for direct comparison with the nonannealed growths. The inset in Fig. 5(a) shows a higher magnification image, featuring the same nanoscale islands previously observed in the nonannealed catalyst underneath the CNTs. Figure 5(b) shows postgrowth low energy Raman spectra of the 1 nm catalyst both with and without a pregrowth anneal, as well as planar monolayer graphene and the bare catalyst for reference.

The preannealed catalyst Raman (green) displays radial breathing mode (RBM) peaks at 210 and 222 cm^{-1}—features typical of CNTs.[53,54] The 1 nm catalyst without preanneal (red) shows radial modes (RMs) at 240 and 271 cm^{-1} that are similar to RBMs, but occur when not all of the eigenvectors point radially inward.[55,56] RMs are common features of "curved" graphene. The peak at 301 cm^{-1} is a SiO_2 peak present in all samples, including the bare catalyst. The planar monolayer graphene is free of any RM or RBM peaks.

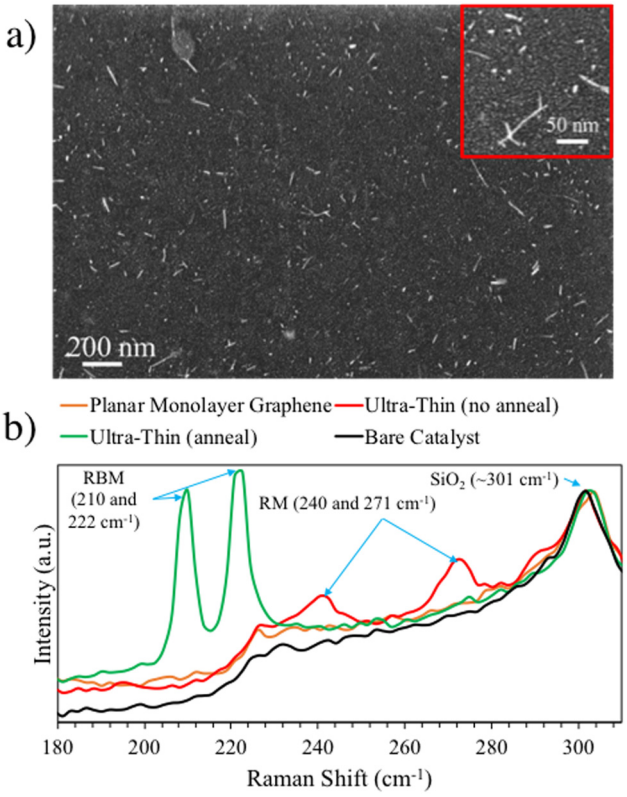

FIG. 5. (a) SEM micrograph of 1 nm catalyst grown for 15 min after a 7 min pregrowth anneal at growth temperature showing growth of carbon nanotube structures, with the inset displaying higher magnification of the same catalyst. (b) Raman spectra comparing typical planar graphene, a 1 nm catalyst grown graphene without an anneal, a 1 nm catalyst grown graphene with an anneal, and the bare catalyst/SiO_2, showing observed RBMs.

The fact that CNTs only appear after first annealing the substrate suggests that they grow from the nanoislands. This is supported by conventional CVD CNT fabrication methods based on nanoparticles.[56,57] If the substrate is not annealed beforehand, there are no separated metal islands for the CNTs to grow from. Instead, a layer of graphene grows on the planar surface. Due to the ultrathin nature of the 1 nm catalyst, the growth is surface-mediated and further graphene layers do not grow. This follows the accepted graphene growth model on Ni-based catalysts, wherein carbon atoms diffuse into the catalyst and precipitate out upon cooling.[41] Here, both the catalyst thinness and the addition of 1 wt. % Au limit the amount of carbon that is able to diffuse into the catalyst, resulting in fewer graphene layers precipitating out upon cooling. This result was also observed in thicker catalysts due to a reduction in nucleation sites such as step edges.[45] In addition to experimentation, simulations have shown the ability of Ni catalysts with added Au to have slightly increased decomposition energies compared to pure Ni, allowing for slower growth and prevention of excessive layering.[46] This number is demonstrably consistent with time, as shown by the consistent Raman characteristics. The lack of a typical metal grain

structure in the ultrathin catalyst also aids in reducing the ultimate layer number of the graphene, as carbon atoms preferentially precipitate at grain boundaries. The ability to produce these consistent curved graphene sheets at 450 °C is made possible by the Ni/Au alloy and by the ultimate thinness of the catalyst.

IV. CONCLUSION

In this research, it has been demonstrated that the implementation of ultrathin multielement catalysts allows for the growth of curved graphene films at low temperatures of 450 °C without the need for a high-temperature preanneal process. These temperatures are far below those required for graphene growth on thicker single element catalysts. It was demonstrated that the mechanism consists of initial graphene growth very quickly upon the surface of the ultrathin catalyst, followed by a breaking up of the catalyst into small metal islands. It was also found that preannealing of the catalyst at the growth temperature produces carbon nanotubes, owing to the morphology of the metal islands. Although the CNT results demonstrated in this report were not optimal, the connection between the formation of graphene and CNTs suggests the importance of the catalyst surface treatment and its thickness in relation to the produced material. Graphene grown on catalysts of ultimate thinness, as demonstrated in this work, presents a potential avenue for methods of growing diffusion barriers and corrosion protection on substrates of arbitrary geometry.

ACKNOWLEDGMENTS

The authors would like to acknowledge that this study is supported in part by the National Science Foundation (NSF) (Award No. 1711994), Intel Corporation, and Oregon Metals Initiative.

REFERENCES

[1]K. S. Novoselov, S. V. Morozov, D. Jiang, Y. Zhang, S. V. Dubonos, I. V. Grigorieva, and A. A. Firsov, Science **306**, 666 (2004).
[2]C. Lee, X. Wei, J. W. Kysar, and J. Hone, Science **321**, 385 (2008).
[3]F. S. Scarpa, S. Adhikari, and A. S. Phani, Nanotechnology **20**, 065709 (2009).
[4]K. I. Bolotin, K. J. Sikes, Z. Jiang, M. Klima, G. Fudenberg, J. Hone, P. Kim, and H. L. Stormer, Solid State Commun. **146**, 351 (2008).
[5]M. Y. Han, B. Özyilmaz, Y. Zhang, and P. Kim, Phys. Rev. Lett. **98**, 206805 (2007).
[6]F. Xia, D. B. Farmer, Y. Lin, and P. Avouris, Nano Lett. **10**, 715 (2010).
[7]H. Cheng, S. Chen, P. Yu, X. Duan, B. Xie, and J. Tian, Appl. Phys. Lett. **103**, 2013112 (2013).
[8]J. Wu, H. A. Becerril, Z. Bao, Z. Liu, Y. Chen, and P. Peumans, Appl. Phys. Lett. **92**, 263302 (2008).
[9]S. Bae *et al.*, Nat. Nanotechnol. **5**, 8 (2010).
[10]C. Liu, Z. Yu, D. Neff, A. Zhamu, and B. Z. Jang, Nano Lett. **10**, 4863 (2010).
[11]H. Kim, K. Y. Park, J. Hong, and K. Kang, Sci. Rep. **4**, 5278 (2014).
[12]T. Maiyalagan, X. Dong, P. Chen, and X. Wang, J. Mater. Chem. **22**, 5286 (2012).
[13]J. Luo, S. Jiang, H. Zhang, J. Jiang, and X. Liu, Anal. Chim. Acta **709**, 47 (2012).
[14]H. J. Yoon, J. H. Yang, Z. Zhou, S. S. Yang, and M. M. C. Cheng, Sens. Actuators B **157**, 1 (2011).
[15]M. G. Chung *et al.*, Sens. Actuators B **166-167**, 172 (2012).
[16]G. S. Kulkarni, K. Reddy, Z. Zhong, and X. Fan, Nat. Commun. **5**, 4376 (2014).
[17]Y. Wang *et al.*, Nano Res. **8**, 1627 (2015).
[18]Y. M. Lin, C. Dimitrakopoulos, K. A. Jenkins, D. B. Farmer, H. Y. Chiu, A. Grill, and P. Avouris, Science **327**, 662 (2010).
[19]Y. M. Lin *et al.*, Science **332**, 1294 (2011).
[20]Y. Wu *et al.*, Nano Lett. **12**, 3062 (2012).
[21]H. Wang, T. Taychatanapat, A. Hsu, K. Watanabe, T. Taniguchi, P. Jarillo-Herrero, and T. Palacios, IEEE Electron Device Lett. **32**, 9 (2011).
[22]E. H. Hwang and S. D. Sarma, Phys. Rev. B **77**, 115449 (2008).
[23]M. Orlita *et al.*, Phys. Rev. Lett. **101**, 267601 (2008).
[24]A. A. Balandin, S. Ghosh, W. Bao, I. Calizo, D. Teweldebrhan, F. Miao, and C. Lau, Nano Lett. **8**, 902 (2008).
[25]Y. Cui, S. I. Kundalwal, and S. Kumar, Carbon **98**, 313 (2016).
[26]W. K. Morrow, S. J. Pearton, and F. Ren, Small **12**, 120 (2016).
[27]S. Stankovich, D. A. Dikin, R. D. Piner, K. A. Kohlhass, A. Kleinhammes, Y. Jia, Y. Wu, S. T. Nguyen, and R. S. Ruoff, Carbon **45**, 1558 (2007).
[28]K. V. Emtsev *et al.*, Nat. Mater. **8**, 203 (2009).
[29]Y. I. Zhang, L. Zhang, and C. Zhou, Acc. Chem. Res. **46**, 2329 (2013).
[30]C. Mattevi, H. Kim, and M. Chhowalla, J. Mater. Chem. **21**, 3324 (2011).
[31]X. Li, C. W. Magnuson, A. Venugopal, R. M. Tromp, J. B. Hannon, E. M. Vogel, L. Colombo, and R. S. Ruoff, J. Am. Chem. Soc. **133**, 2816 (2011).
[32]S. Bhaviripudi, X. Jia, M. S. Dresselhaus, and J. Kong, Nano Lett. **10**, 4128 (2010).
[33]W. Liu, H. Li, C. Xu, Y. Khatami, and K. Banerjee, Carbon **49**, 4122 (2011).
[34]K. S. Kim *et al.*, Nature **457**, 706 (2009).
[35]Y. Zhang, L. Gomez, F. N. Ishikawa, A. Madaria, K. Ryu, C. Wang, A. Badmaev, and C. Zhou, J. Phys. Chem. Lett. **1**, 20 (2010).
[36]H. J. Park, J. Meyer, S. Roth, and V. Skákalová, Carbon **48**, 1088 (2010).
[37]J. Sun, N. Lindvall, M. T. Cole, K. T. Angel, T. Wang, K. B. Teo, D. H. Chua, J. Liu, and A. Yurgens, IEEE Trans. Nanotechnol. **11**, 2 (2012).
[38]M. Qi, Z. Ren, Y. Jiao, Y. Zhou, X. Xu, W. Li, J. Li, X. Zheng, and J. Bai, J. Phys. Chem. C **117**, 27 (2013).
[39]B. Zhang, W. H. Lee, R. Piner, I. Kholmanov, Y. Wu, H. Li, H. Ji, and R. S. Ruoff, ACS Nano **6**, 2471 (2012).
[40]Q. Yu, J. Lian, S. Siriponglert, H. Li, Y. P. Chen, and S. S. Pei, Appl. Phys. Lett. **93**, 113103 (2008).
[41]B. Dai, L. Fu, Z. Zou, M. Wang, H. Xu, S. Wang, and Z. Liu, Nat. Commun. **2**, 522 (2011).
[42]R. S. Weatherup, B. C. Bayer, R. Blume, C. Ducati, C. Baehtz, R. Schlogl, and S. Hofmann, Nano Lett. **11**, 4154 (2011).
[43]W. Regan, N. Alem, B. Alemán, B. Geng, Ç. Girit, L. Maserati, F. Wang, M. Crommie, and A. Zettl, Appl. Phys. Lett. **96**, 113102 (2010).
[44]E. Auchter, J. Marquez, S. L. Yarbro, and E. Dervishi, AIP Adv. **7**, 125306 (2017).
[45]J. Tracy, O. Zietz, S. Olson, and J. Jiao, Nanoscale Res. Lett. **14**, 335 (2019).
[46]H. Zhan, B. Jiang, O. Zietz, S. Olson, and J. Jiao, Mater. Res. Express **7**, 015603 (2019).
[47]C. Wang, B. Xiao, and Y. H. Ding, New J. Chem. **37**, 3 (2013).
[48]F. Tuinstra and J. L. Koenig, J. Chem. Phys. **53**, 1126 (1970).
[49]A. C. Ferrari *et al.*, Phys. Rev. Lett. **97**, 187401 (2006).
[50]A. C. Ferrari and D. M. Basko, Nat. Nanotechnol. **8**, 235 (2013).
[51]T. M. G. Mohiuddin *et al.*, Phys. Rev. B **79**, 205433 (2009).
[52]J. Zabel, R. R. Nair, A. Ott, T. Georgiou, A. K. Geim, K. S. Novoselov, and C. Casiraghi, Nano Lett. **12**, 617 (2012).
[53]J. Maultzsch, H. Telg, S. Reich, and C. Thomsen, Phys. Rev. B **72**, 205438 (2005).
[54]J. Kürti, V. Zólyomi, M. Kertesz, and G. Sun, New J. Phys. **5**, 125 (2003).
[55]J. K. Lee, K. P. S. S. Hembram, Y. Park, S. G. Lee, J. G. Kim, W. Lee, and D. J. Moon, J. Phys. Chem. Lett. **8**, 2597 (2017).
[56]R. Podila, R. Rao, R. Tsuchikawa, M. Ishigami, and A. M. Rao, ACS Nano **6**, 5784 (2012).
[57]S. B. Sinnott, R. Andrews, D. Qian, A. M. Rao, Z. Mao, E. C. Dickey, and F. Derbyshire, Chem. Phys. Lett. **315**, 25 (1999).